



1 Multidecadal behavior of the North Atlantic Oscillation during 2 the last millennium

3 Andrew A. Flaim¹, Bronwen L. Konecky¹, Sloan Coats²

4 ¹Department of Earth, Environmental, and Planetary Sciences, Washington University in St. Louis, St. Louis, MO,
5 USA

6 ²Department of Earth Sciences, University of Hawai'i at Mānoa, Honolulu, HI, USA

7 *Correspondence to:* Andrew A. Flaim (aflaim@wustl.edu)

8 **Abstract.** The North Atlantic Oscillation (NAO) is a major source of atmospheric variability in the North-
9 ern Hemisphere, affecting temperature, precipitation, and storm tracks across North America and Eurasia.
10 Understanding NAO variability on multidecadal to centennial timescales requires paleo-reconstructions,
11 but previously published reconstructions disagree on the magnitude of low-frequency NAO variability over
12 the last millennium. Paleoclimate proxies for the oxygen and hydrogen isotope composition of meteoric
13 waters have thus far been under-utilized in published NAO reconstructions. Here, we present a new recon-
14 struction of the NAO over the last millennium using the Iso2k database, a collection of globally distributed
15 water isotope-based paleoclimate proxy records. In contrast to recent NAO reconstructions, we find signif-
16 icant multidecadal to centennial scale variability. Critically, however, the strength of the low-frequency
17 signal has not been consistent throughout the last millennium. Isotope-enabled model simulations did not
18 reproduce the low-frequency signal in the NAO reconstructions and thus it may be necessary to account for
19 low-frequency variability when projecting the impacts of the NAO on temperature and precipitation under
20 future climate scenarios.

21 1.0 Introduction

22 Weather and climate in Europe, Greenland, and eastern North America are heavily influenced by the North
23 Atlantic Oscillation (NAO), which is associated with the dominant pattern of sea level pressure variability
24 in the North Atlantic. The NAO is responsible for variability and extremes in both temperature and hydro-
25 climate across the region (Casanueva et al., 2014; Hurrell, 1995; Hurrell and Deser, 2009; Trigo et al., 2002;
26 Villarini et al., 2011; Zanardo et al., 2019), so better understanding it and its connections to temperature
27 and precipitation is critical for contextualizing past and future climate changes.

28 The NAO index is typically defined as the difference between the normalized winter sea-level pressures in
29 Stykkishólmur, Iceland, and Gibraltar (Jones et al., 1997; Vinther et al., 2003a). The index is a proxy for
30 coherent large-scale patterns of atmospheric circulation. For instance, during positive NAO conditions the
31 North Atlantic Jet is deflected northwards, driving warm and wet winters over northern Europe and eastern
32 North America contrasted by cool and dry winters in the Mediterranean. The opposite patterns are observed
33 during negative NAO conditions (Hurrell, 1995; Hurrell and Deser, 2009; Woollings et al., 2010, 2018;
34 Woollings and Blackburn, 2012).

35 Europe is home to some of the longest continuous instrumental records of sea level pressure, extending
36 back through 1823 CE (Jones et al., 1997; Vinther et al., 2003a). However, even these long records provide
37 only a limited perspective on the low frequency (multidecadal to centennial timescale) variability of the
38 NAO, timescales that are critical for contextualizing and understanding its response to anthropogenic emis-
39 sions (Cook et al., 2019; Woollings et al., 2015). Additionally, the instrumental records underlying indices
40 for the NAO are focused on Europe and the eastern North Atlantic, and thus are more limited in capturing
41 NAO impacts further up- (e.g., North America and Greenland) and down-stream (e.g., Eurasia) (e.g. Felis



et al., 2000; Liu et al., 2018; Xiaoge et al., 2010). Instrumental data for the NAO outside of the North Atlantic region is especially limited in duration and coverage, so paleoclimate proxy-based reconstructions are a valuable tool for characterizing the NAO and its impacts on timescales that extend beyond the instrumental record, and outside the regions where long instrumental records of sea level pressure exist.

Substantial disagreements still exist between published reconstructions of the NAO index, especially on the nature of multidecadal to centennial scale variability during the last millennium (Cook et al., 2019; Schmutz et al., 2000). Geologic archives such as tree-ring width chronologies, speleothems, glacier ice, and lake sediments have been employed to investigate paleo-signals of the NAO (Baldini et al., 2008; Brittingham et al., 2019; Cook et al., 2002; Hernández et al., 2020; Kozachek et al., 2017; Kuhnert et al., 2005; Lehner et al., 2012; Michel et al., 2020; Ortega et al., 2015; Sánchez-López et al., 2016; Sorrel et al., 2007; Trouet et al., 2009; Vinther et al., 2003b). However, these published reconstructions suggest a wide range of NAO variability across timescales from higher relative variance at low frequencies (e.g., Ortega et al. 2015) to nearly equal variance at all frequencies (e.g., Cook et al., 2019). Properly constraining low-frequency variability in the NAO is critical not only for future projections, but also for establishing the mechanisms and drivers of the NAO across timescales.

Understanding discrepancies in the published reconstructions is complicated by the different proxy types used as predictors, which may bring their own inherent spectral biases. Ice cores, tree rings, and speleothems, for instance, have each been shown to exhibit unique spectral biases (Dee et al., 2017; Franke et al., 2013). Drought-sensitive tree-ring reconstructions, which have been used extensively in reconstructions of the NAO, can exhibit substantial autocorrelation (Alley, 1984; Ault et al., 2013). Only a small fraction of the proxy records included in published NAO reconstructions are based on the stable oxygen or hydrogen isotopic compositions of environmental waters like precipitation, seawater, lake water, or soil and groundwater (hereafter called water isotopes). Water isotopes provide information about the NAO on broader spatial and temporal scales than other proxies because they integrate information on basin-wide to hemispheric scales that is otherwise overprinted by regional or site-specific noise (Moerman et al., 2013). Water isotope-based proxies therefore offer a valuable new perspective on the NAO during the last millennium.

Water isotopes have long been used as integrative tracers of the modern water cycle because they are modified by fractionation processes in which the rare heavy isotopologues of water (e.g., H_2^{18}O , H^{18}O) fractionate from their lighter, more common counterpart (H_2^{16}O) during evaporation, condensation, and other phase changes (Bowen et al., 2019; Dansgaard, 1964; Galewsky et al., 2016; Rozanski et al., 1993). The ratios of the heavy to light isotopes, relative to Standard Mean Ocean Water, are represented by $\delta^{18}\text{O}$ for oxygen and δD for hydrogen. We focus on $\delta^{18}\text{O}$ because the records in our analysis are predominantly based on oxygen isotope measurements. These water isotope ratios can be used to track phase changes as the water moves through and among oceans, the atmosphere, and land (e.g., Bowen et al., 2019; Galewsky et al., 2016; Gat, 2010; Rozanski et al., 1993). Water isotopes are more closely correlated with major modes of variability than precipitation amount, for example, because the majority of diurnal to interannual rainfall $\delta^{18}\text{O}$ ($\delta^{18}\text{O}_{\text{precip}}$) variability originates from regional scale hydrological processes like convective intensity, moisture transport history, and moisture source changes (Moerman et al., 2013). Isotope values at a particular location are often linked to teleconnections far afield from the measurement site, highlighting the value of water isotope proxy records for evaluating regional to continental scale phenomena (Puntsag et al., 2016; Vachon et al., 2010; Vuille and Werner, 2005). Therefore, water isotope observations and proxy data may provide useful information about the NAO, even outside the immediate centers of action in the North Atlantic.

Within Europe, previous studies have demonstrated that the NAO is responsible for changes in $\delta^{18}\text{O}_{\text{precip}}$ by comparing the NAO index with instrumental $\delta^{18}\text{O}_{\text{precip}}$ measurements (Baldini et al., 2008; Comas-Bru et



al., 2016; Deininger et al., 2016; Langebroek et al., 2011). For example, the continental effect, or the “distance from the coast” effect, is the gradient in amount-weighted $\delta^{18}\text{O}_{\text{precip}}$ across the continent, where $\delta^{18}\text{O}_{\text{precip}}$ becomes more negative further inland (Dansgaard, 1964). The slope of this continental effect depends on the winter NAO as a function of atmospheric temperature and precipitation (Comas-Bru et al., 2016; Deininger et al., 2016; Hurrell, 1995). Specifically, steeper air temperature gradients across the continent, in combination with decreased atmospheric water content in the continental interior relative to the coasts, drive steeper observed $\delta^{18}\text{O}$ west-east gradients across northern Europe during negative winter NAO phases (Deininger et al., 2016; Trigo et al., 2002).

Changes in the moisture source or transport pathway may also influence $\delta^{18}\text{O}_{\text{precip}}$ by altering patterns of rainout. In Greenland, for example, moisture source and transport models have been applied to diagnose the effects that changes in atmospheric circulation and moisture source locations have on $\delta^{18}\text{O}_{\text{precip}}$ during different phases of the NAO (Sodemann et al., 2008). Simulated water isotope ratios of Greenland precipitation had higher (lower) $\delta^{18}\text{O}$ values during a positive (negative) NAO, as moisture was primarily drawn from the seas north of Iceland (the southwestern North Atlantic). Ice core tops collected from the central region of the ice sheet support these results, although the models suggested spatial heterogeneity that may not be captured by the relatively limited distribution of ice cores (Sodemann et al., 2008). These initial studies demonstrate mechanistic links between the NAO and water isotopes, but existing reconstructions of the NAO have not yet made full use of water isotope-based proxy records.

Here we reconstruct the NAO index for the last millennium (1000–2000 CE) using $\delta^{18}\text{O}$ and δD proxies from the PAGES Iso2k database, a global compilation of water isotope-based records spanning the Common Era (Konecky et al., 2020). The global coverage of this database allows us to identify water isotope relationships with the NAO in its centers of action (Greenland and western Europe) and further afield (e.g., the Himalayas and Tibetan Plateau). We evaluate the reconstruction with the instrumental NAO index (Vinther et al., 2003a), observed $\delta^{18}\text{O}_{\text{precip}}$ in the Global Network of Isotopes in Precipitation database (GNIP; IAEA/WMO, 2008), and climate model output from the isotope-enabled Last Millennium Ensemble of the Community Earth System Model (iCESM iLME; Brady et al., 2019). In particular, the isotope-enabled simulations allow us to infer how NAO-induced changes in temperature, precipitation, and moisture transport pathways translate to $\delta^{18}\text{O}_{\text{precip}}$, and therefore how GNIP stations and water isotope proxies in the Iso2k database record the NAO.

2.0 Methods

2.1 Datasets

Four datasets were used herein: the Vinther et al. (2003) instrumental NAO index ($\text{NAO}_{\text{Vinther}}$), the PAGES Iso2k database (Konecky et al., 2020), the GNIP database containing modern isotope measurements in rainfall (IAEA/WMO, 2008), and the iCESM iLME (Brady et al., 2019).

The Iso2k database is a collection of previously published proxy $\delta^{18}\text{O}$ and δD records including ice cores, speleothems, and wood cellulose, that span the Common Era (0–2000 CE). Although the database contains proxies for oceanic conditions, only terrestrial Northern Hemisphere records were used here to focus on the atmospheric components of the NAO, and to most directly compare with modeled atmospheric variables associated with the NAO. Furthermore, only records that had at least annual resolution and 33% data coverage in the calibration interval between 1823 and 2000 CE were included. The 33% data coverage threshold was selected after extensive experiments using different time intervals and data coverage thresholds in attempts to balance the inclusion of records in the analysis while minimizing the influence of missing data. Increasing the data coverage requirement above 33% dramatically cut the number of included records and limited the spatial coverage of the analysis, while lower thresholds permitted inclusion of records with large



sections of missing data. Adjusting the bounds of the time interval also changed the records included in the analysis. However, few Iso2k records have data extending into years more recent than 2000 CE (Konecky et al., 2020), and the $\text{NAO}_{\text{vinther}}$ index becomes less constrained by observational data before 1823 CE.

The GNIP database contains measurements of both $\delta^{18}\text{O}$ and δD in precipitation. We only use $\delta^{18}\text{O}$ for our analyses as δD data from stations are less commonly available or discontinuous. Only sites with at least 10 winters of data were included (not necessarily consecutive), based on the general statistical principle that no fewer than 10 data points should be used to establish a linear relationship (Pearson, 1901). Any sub-monthly data were converted to monthly means following Putman and Bowen (2019), and the monthly $\delta^{18}\text{O}$ was then averaged to boreal winter (December-January-February—DJF) seasonal means after amount-weighting using the precipitation amount data from each site.

Finally, three fully forced (i.e., with all transient external forcings) iCESM iLME simulations, each spanning 850–2005 CE, were used to evaluate the spatial relationships of $\delta^{18}\text{O}_{\text{precip}}$, temperature, and precipitation with the NAO. The iLME uses a ~ 2 -degree atmosphere and land and ~ 1 -degree ocean and sea ice version of the respective model components. Monthly mean values for sea level pressure, surface air temperature, total precipitation, wind vectors, specific humidity, and $\delta^{18}\text{O}_{\text{precip}}$ were analyzed herein. Vertically integrated water vapor transport (IVT) was calculated by weighting the monthly mean wind vectors by monthly specific humidity and summing over the full atmospheric column. The winter (DJF) NAO index was defined in the iLME as the difference between the averaged sea level pressure in grid cells containing Reykjavik, Iceland (65°N , 22°W) and Ponta Delgada, Spain (38°N , 25°W). This index (NAO_{iLME}) was then regressed against DJF sea level pressure, surface air temperature, total precipitation, and $\delta^{18}\text{O}_{\text{precip}}$ in the iLME to produce spatial correlation maps of these variables with the NAO. Years with positive and negative NAO events are defined as those with winter NAO_{iLME} index values greater and less than one standard deviation from the mean, respectively.

2.2 NAO signals in Iso2k

Iso2k records were annualized by averaging any sub-annual data into a standard January-December year, again following Putman and Bowen (2019). Each record was standardized to anomaly units by subtracting the mean and dividing by the standard deviation of the full series. This allowed comparisons between oxygen and hydrogen isotope records, as well as between records collected from archive types with differing climate sensitivities.

A composite-plus-scale (CPS) reconstruction approach was applied to extract the signal of the NAO from the Iso2k records. The CPS ensemble was produced using methods mirroring those applied by previous studies with similar goals (Mann et al., 2008; Neukom et al., 2014). For each member of the 1000-member ensemble, 15% of the Northern Hemisphere Iso2k records (Section 2.1) were randomly removed. The CPS reconstruction was then done by normalizing and scaling the remaining records according to their correlation with the $\text{NAO}_{\text{vinther}}$ index in the calibration interval from 1873–2000 CE and then computing the mean of the records at each timestep. The mean and variance of the resulting composite was then normalized to match that of the $\text{NAO}_{\text{vinther}}$ index. The correlation of the reconstruction ensemble members was tested against the first 50 years of the $\text{NAO}_{\text{vinther}}$ index as the validation interval from 1823–1873 CE. Results were not sensitive to the duration and timing of the calibration and validation intervals.

A null hypothesis was developed by constructing an ensemble of first-order autoregressive (AR(1)) noise records. Noise records corresponding to the Iso2k records above were produced and then composited and scaled using the same CPS methods. The correlation of the resulting composite was then tested against the $\text{NAO}_{\text{vinther}}$ index. This process was repeated one hundred times to produce a range of correlations that might be expected from one hundred “reconstructions” of the NAO using autocorrelated noise.



To test the relative influence of records outside of the NAO centers of action on our reconstruction, the same CPS procedures were performed on only records from Greenland and Europe and separately on records from the Indo-Asian monsoon region (Fig. 1, blacked dashed regions). The results were compared with the full reconstruction, and, to ensure the high skill of the full reconstruction was not simply the result of having more records, the CPS procedure was performed using records from the regional subsets after adding autocorrelated noise records to bring the total number of records equal to the full reconstruction (“noise-padded”; Fig. S1).

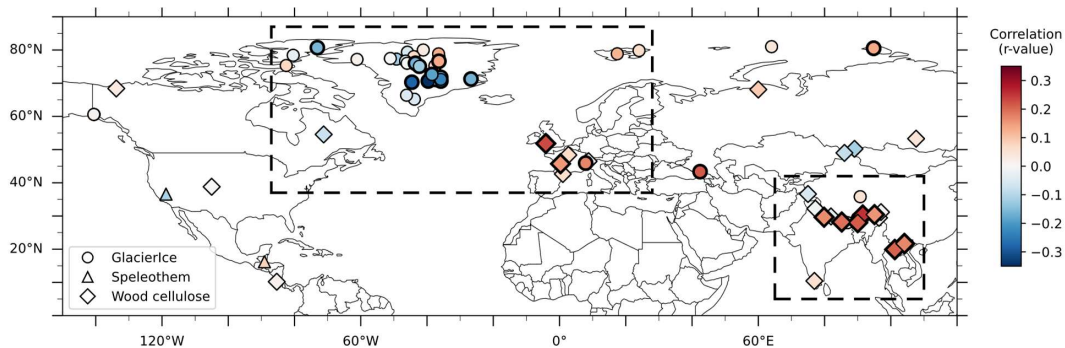


Figure 1. Map of Iso2k records included in the analysis. Shapes correspond to archive type and colors denote the Pearson’s r -value of each record with $NAO_{vinther}$ (1823–2000 CE). Bold outlines signify significant correlation ($p < 0.1$). Regional subsets used for validation indicated by dashed boxes over Greenland and southeast Asia.

Spectral decomposition of the full NAO reconstruction was completed using the multi-taper method (Thomson, 1982) through the R package *geoChronR*, which in turn leverages the *astrochron* R package (Mckay et al., 2020; Meyers, 2012). The resulting decomposition was compared against an AR(1) null hypothesis (e.g., Zhu et al. 2019). Wavelet analysis was performed using the R package ‘WaveletComp’ (Roesch and Schmidbaur, 2018). This method allows for an investigation of changes in the frequency of signals through time. Wavelet analysis was applied to the full reconstruction as well as the reconstructions based on regional subsets. Wavelet analysis was also performed on reconstructions produced from only a single proxy type to investigate the impact that record availability and proxy type had on the spectral characteristics of the reconstructions.

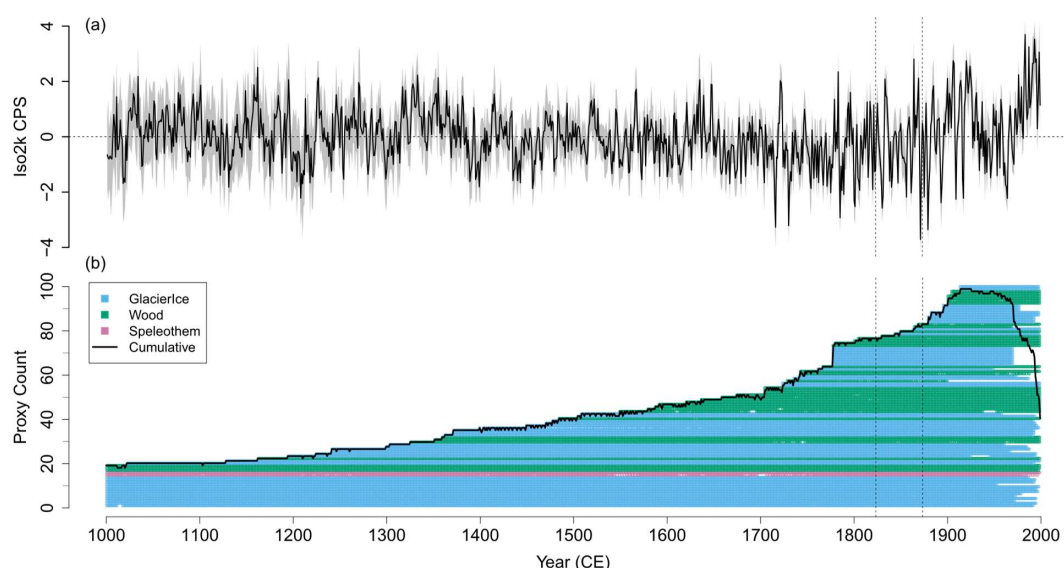
3.0 Results

3.1 NAO-correlated Iso2k records and CPS reconstructions

A total of 92 records from Iso2k were extracted from the Northern Hemisphere with at least annual resolution and 33% coverage between 1823 and 2000 CE. This included 2 speleothems, 36 wood cellulose, and 50 glacier ice records, with all records based on $\delta^{18}O$ except three glacier ice records of δD . Pearson correlation r -values of these records with the $NAO_{vinther}$ index ranged from -0.37 to 0.29. Thirty-six of the original 92 proxy records were significantly correlated (p -value < 0.1) with $NAO_{vinther}$ in the calibration interval including 15 wood cellulose, and 21 glacier ice records. Records with significant correlations spanned the full spatial distribution of the original 92 records, including glacier ice records in Greenland, the Alps, and the Himalayas, and wood cellulose in Europe, northern India, and the Tibetan Plateau (Fig. 1, bold



207 symbols). A total of 19 records spanned the full last millennium including 14 glacier ice, 3 wood cellulose,
208 and 2 speleothem records (Fig. 2b), of which only 6 glacier ice records were significantly correlated with
209 the NAO_{Vinter} index (Fig. S2).



210
211 **Figure 2.** (a) NAO reconstruction ensemble members (grey shading) and ensemble median (black line).
212 Horizontal dashed line shows zero. Vertical dashed lines indicate calibration and validation cutoff years at
213 1823 CE and 1873 CE. (b) Record coverage through time for the full Northern Hemisphere Iso2k dataset
214 including glacier ice (blue), wood cellulose (green), and speleothem (red) records. Solid black line indi-
215 cates the total number of available records in each year.

216
217 The median of the ensemble of reconstructions ranged from approximately -3.7 to 3.7, while the full en-
218 semble spanned from -4.3 to 4.2 (Fig. 2a). The ensemble members were all significantly ($p < 0.001$) posi-
219 tively correlated with the NAO_{Vinter} index during the validation interval from 1823–1873 CE, with corre-
220 lation values ranging from 0.34 to 0.56 and a median of 0.47 (Fig. 3, red).

221 Restricting the spatial extent of records included in the reconstruction to only Greenland and Europe pro-
222 duced a substantial decrease in correlations with the NAO_{Vinter} index during the validation interval, with
223 correlation values between 0.27 to 0.47, and a median of 0.37. (Fig. 3, blue). Using only records from
224 northern India and the Tibetan plateau in the reconstructions produced a median validation correlation value
225 of 0.44 (with values ranging from 0.27 to 0.51) that exceeded the Greenland and Europe-only recon-
226 structions (Fig. 3, black). Using the two regions together produced the reconstructions with the highest median
227 correlation at 0.49, with individual ensemble values ranging from 0.39 to 0.62 (Fig. 3, green), slightly higher
228 than even reconstructions using all 92 records (Fig. 3, red). Padding the regional reconstructions with au-
229 tocorrelated noise did not improve their validation correlations, suggesting the skill of the full Northern
230 Hemisphere reconstruction was not simply a function of the large number of records (Fig. S1). The high
231 skill of the two regions combined highlights the importance of including records outside the center of action
232 of the NAO index.

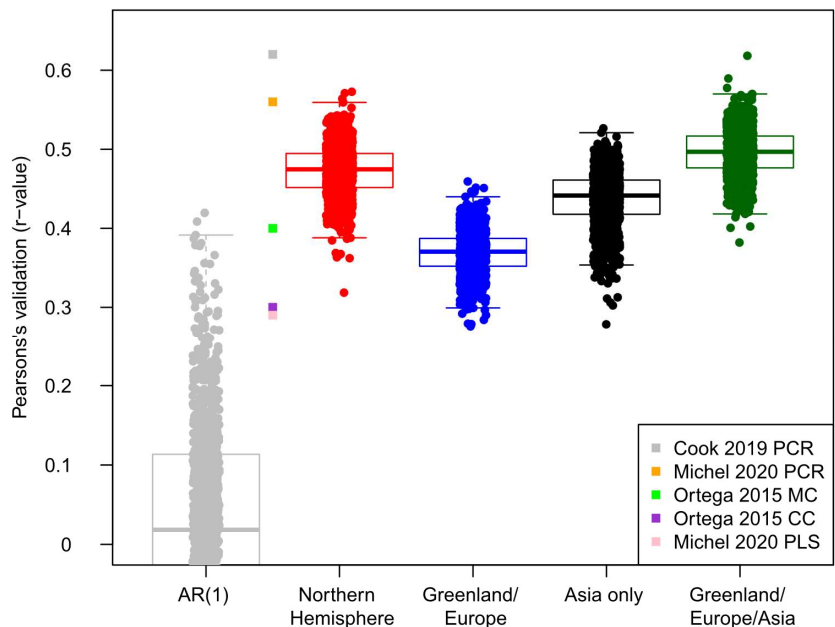


Figure 3. Box and whisker plots of validation (1823–1873 CE) metrics for the reconstructions using first-order autocorrelated noise (grey), the Northern Hemisphere Iso2k dataset seen in Fig. 1 (red, n=92), only records from Greenland and Europe (blue, n=47), only records from southeast Asia and the Tibetan Plateau (black, n=27), and the combination of Greenland, Europe, southeast Asia, and the Tibetan plateau (green, n=74). Regional subsets correspond with dashed boxes in Fig. 1. Individual colored squares indicate validation scores for other published NAO reconstructions.

3.2 NAO fingerprints in GNIP isotope stations

Of the 1005 stations extracted from the GNIP database, 146 stations met conditions of at least 10 non-consecutive winter (DJF) seasons of data (Fig. 4 symbols) and of those, 50 had a significant ($p < 0.1$) correlation with the $NAO_{vinther}$ index (Fig. 4, symbols with bold outlines). Of those 50 stations, 47 were positively correlated with the NAO, with Pearson's R values ranging from 0.29 to 0.86, while 3 were negatively correlated, ranging from -0.34 to -0.53. The positively correlated stations were concentrated in central Europe, although several stations were also positively correlated in Finland, the Azores, Barbados, and Greece. The negatively correlated stations were in Iceland, southwest Russia, and Turkey. The correlation dipole between the Iceland station and the stations in Europe is broadly consistent with the sea level pressure (SLP) dipole that is characteristic of the NAO, in which the NAO is negatively correlated with SLP over Iceland and positively correlated over Europe (Fig. S3). This pattern is also consistent with past studies of $\delta^{18}O$ correlations with the NAO (Deininger et al., 2016).

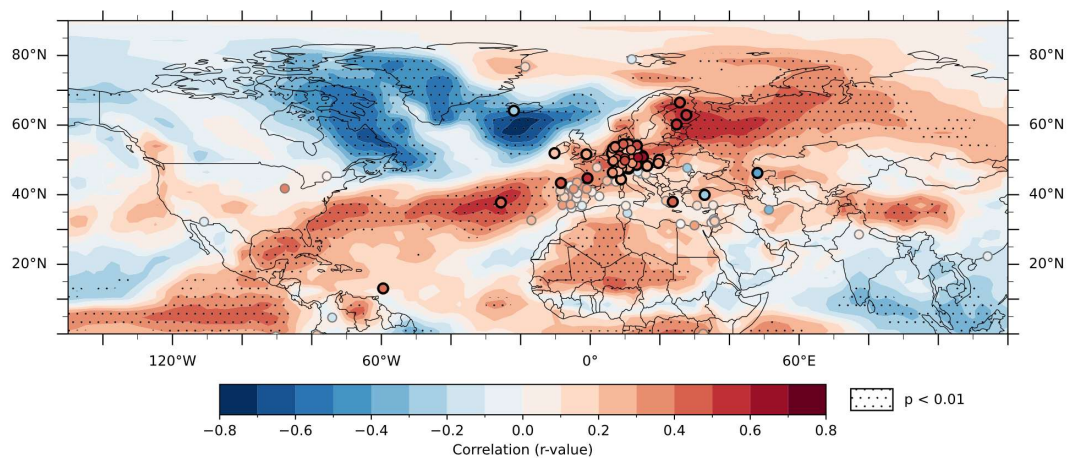
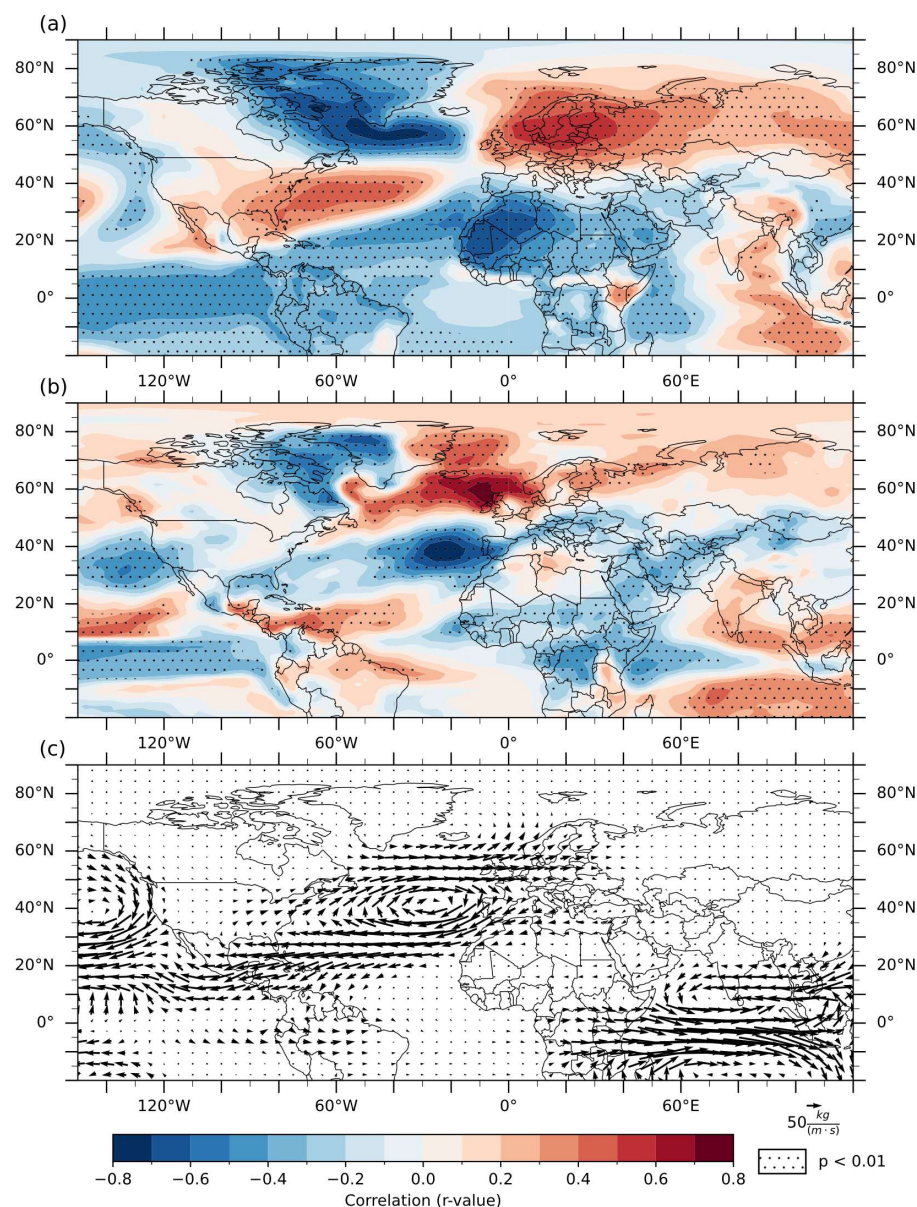


Figure 4. Winter NAO_{iLME} correlations (color contours) with $iLME$ winter $\delta^{18}O_{precip}$ from 1823–2000 CE. Stippling denotes $p < 0.01$. Symbols show GNIP stations with ≥ 10 winters colored by $\delta^{18}O_{precip}$ correlations with $NAO_{Vinther}$, bold symbols show significant ($p < 0.1$) correlations.

3.3 NAO fingerprints in the iLME

The winter (DJF) NAO_{iLME} index values ranged from -5.29 to 3.15 with a standard deviation of 1.79 through the period 1823–2000 CE (Fig. S4a). As with the $NAO_{Vinther}$ index, the winter NAO_{iLME} was slightly positively skewed, but with more extreme values during negative years (Fig. S4b-c). The NAO_{iLME} captured the main spatial features of observed NAO impacts in the North Atlantic region, with similar correlations to SLP, temperature, and precipitation (Compo et al., 2011; Hernández et al., 2020). Correlations between NAO_{iLME} and winter precipitation amount were less spatially extensive than with temperature (Fig. 5a-b). However, the precipitation correlations with the NAO_{iLME} showed an east/west contrast over Greenland, with positive correlations in the east and negative correlations spanning western Greenland and the northeastern Canadian Arctic. This differs notably from the 20th Century Reanalysis correlations, in which no significant NAO-precipitation correlations were found over Greenland (Hernández et al., 2020). Positive winter NAO_{iLME} years were characterized by greater IVT from the North Atlantic and stronger anticyclonic flow in the subtropical Atlantic, which increases moisture transport from the North Atlantic into Northern Europe and Scandinavia relative to negative winter NAO_{iLME} years, consistent with a stronger and more northern jet (Fig. 5c).

Winter NAO_{iLME} correlations with amount-weighted $\delta^{18}O$ of winter precipitation ($\delta^{18}O_{precip}$) were negative over western Greenland and Iceland, and positive over Europe, Scandinavia, and the mid-latitude North Atlantic (Fig. 4, shading). The NAO_{iLME} index was also positively correlated with winter $\delta^{18}O_{precip}$ over the tropical Pacific, west Africa, and the Tibetan plateau. Although GNIP $\delta^{18}O_{precip}$ observations are limited, and nonexistent over the oceans, the correlations were consistent with the available GNIP $\delta^{18}O_{precip}$ data (Fig. 4, symbols).



279

280 **Figure 5.** Winter NAO_{ILME} correlations (color contours) with iLME winter surface air temperature,
 281 precipitation amount, and composite IVT from 1823–2000 CE. Stippling denotes $p < 0.01$. (a) NAO_{ILME}
 282 correlation with winter surface air temperature. (b) NAO_{ILME} correlation with winter precipitation amount.
 283 (c) Difference between winter IVT during positive and negative winter NAO_{ILME} years, defined as NAO_{ILME}
 284 greater or less than one standard deviation from the mean, respectively, over the period 1823–2000 CE.

285



3.4 Spectral analysis of the NAO reconstructions and the NAO in the iLME

Wavelet decomposition of the NAO reconstruction found significant ($p < 0.05$) power in four main “bands” throughout the last millennium, which here we refer to as interannual (1–10 years), decadal (10–30 years), multidecadal (30–100 years), and centennial (100+ years; Fig. 6a). The multi-taper method spectral decomposition of the full reconstruction over the last millennium showed higher power at longer periods (Fig. 6b). Peaks that rose above the 95% confidence level occurred in the interannual band (2–6 years), as well as at decadal, multidecadal, and centennial scales (11, 23, 94, and 300+ years). The NAO reconstruction had significant power in the interannual and decadal bands from the early 1700s through present (Fig. 6a). Power in the interannual band was weaker prior to 1550 CE. Significant decadal and multidecadal power also persisted from ca. 1000–1300 CE, despite being mostly absent by the mid-millennium. Significant multidecadal to centennial power extended throughout the full reconstruction, although with lower power than the higher frequency bands.

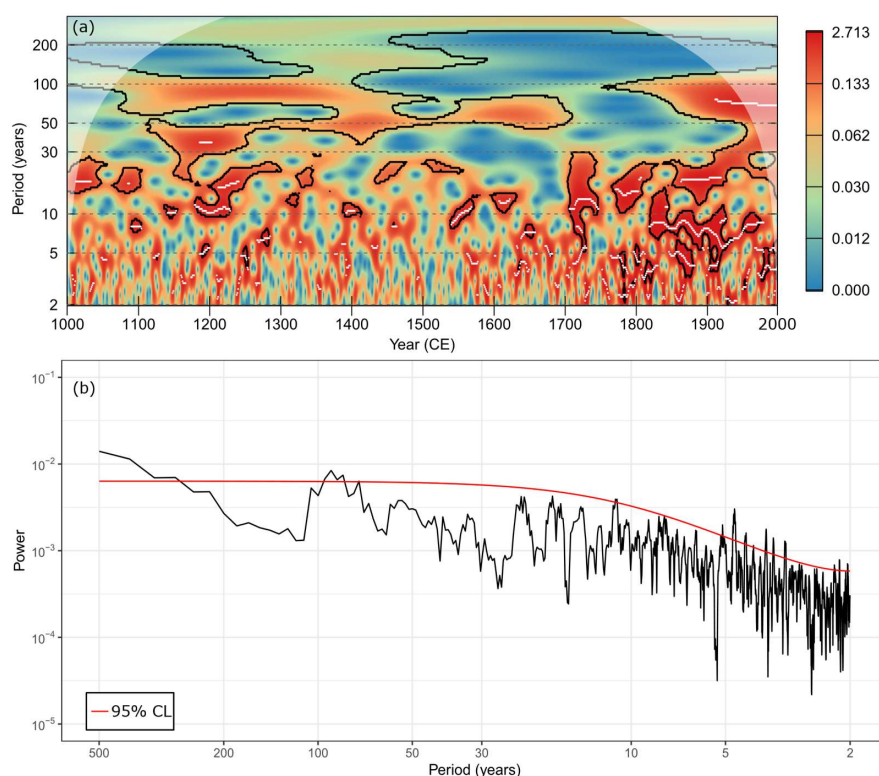
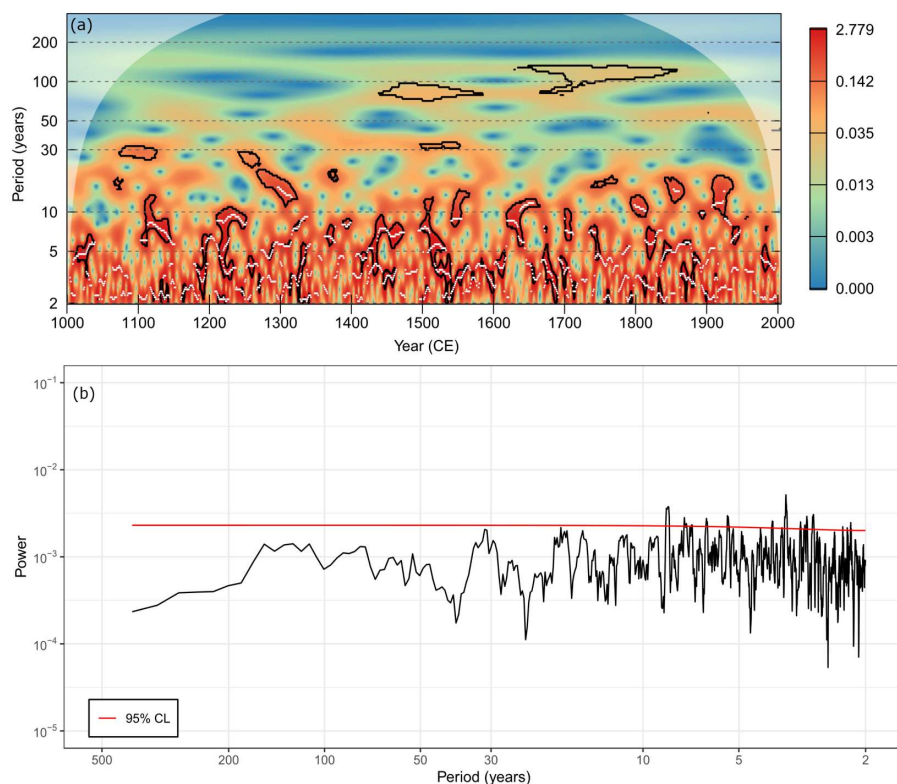


Figure 6. (a) Wavelet decomposition of the NAO reconstruction from 1000–2000 CE. Color contours are scaled by power quantiles. Black contours bound statistically significant power ($p < 0.05$) and white curves show ridges (power maxima). White envelope shows the region of influence where padding may influence estimates. (b) The multi-taper method spectral decomposition for the NAO reconstruction. Red line shows 95% confidence level based on an AR(1) null.



To investigate the impacts of proxy type on the spectral character of the reconstruction we repeated the wavelet and multi-taper analysis twice: First using a reconstruction based only on glacier ice records, and again with a reconstruction using only wood cellulose records (Fig. S5). Like the full reconstruction, both proxy-specific reconstructions exhibited significant interannual to decadal power, but glacier ice records had higher multidecadal to centennial power than wood cellulose records.

The reconstruction using glacier ice records had consistent significant power across scales from the late 1700's through present and from 1000 to about 1250 CE (Fig. S5a). Nevertheless, the mid-millennium had only intermittent significant power on interannual to decadal scales. By contrast, power on multidecadal and centennial scales was notably weaker in the later part of the millennium in the reconstructions using wood cellulose records. While these reconstructions had significant power in the interannual to decadal band from about 1600–2000 CE (Fig. S5b), limited availability of wood cellulose records prior to 1600 CE means the wavelet decomposition was based only on a small number of records and likely not reliable (Fig. 2b).



318

319 **Figure 7.** As in Fig. 6 but for the NAO_{ILME}.

320

321 The wavelet decomposition of NAO_{ILME} exhibited characteristics that were largely distinct from any of the
322 reconstructions. Specifically, interannual variability dominated the NAO_{ILME} over the last millennium, with
323 the only significant (and still relatively weak) decadal power early in the millennium (Fig. 7a). The multi-



taper method decomposition of the NAO_{iLME} confirmed the lack of multidecadal and centennial scale power (Fig. 7b) and the generally ‘white noise’ character of NAO_{iLME} with several significant inter-annual peaks (2-8 years) but overall low power at lower frequencies.

4.0 Discussion

4.1 Regionally variable drivers of $\text{NAO}-\delta^{18}\text{O}_{\text{precip}}$ relationships in Europe

There is a clear imprint of the NAO on records in the Iso2k database. Opposing positive and negative correlations in northern Europe and southern Greenland, respectively, are consistent with the observed contrast in temperature and precipitation associated with the winter NAO (Fig. 1; Hernández et al., 2020). Correlations between the NAO and observed and modeled $\delta^{18}\text{O}_{\text{precip}}$ suggest that the temperature effect is a major control on these relationships, especially at high latitudes in western Greenland, northern Europe, and Scandinavia (Fig. 4, 5a). Specifically, warm air temperatures over northern Europe during a positive NAO cause weaker temperature-dependent Rayleigh fractionation during condensation and decreased rainout along the westerly path of distillation, while cool air temperatures during negative NAO cause stronger Rayleigh fractionation and increased rainout (Dansgaard, 1964), all of which should produce a positive $\delta^{18}\text{O}_{\text{precip}}/\text{NAO}$ relationship. However, temperature is clearly not the only mechanism by which the NAO influences $\delta^{18}\text{O}_{\text{precip}}$. Globally, in locations where a precipitation “amount effect” is observed (particularly, though not exclusively, at low latitudes), the amount of precipitation is inversely correlated with $\delta^{18}\text{O}_{\text{precip}}$ (Nusbaumer et al., 2017). The NAO impacts precipitation amounts in both Europe and Greenland by redirecting storm tracks in the Atlantic (Hurrell, 1995; Hurrell and Deser, 2009; Woollings et al., 2010, 2018; Woollings and Blackburn, 2012). Unlike temperature, precipitation amount-driven impacts of the NAO would therefore yield a negative correlation with $\delta^{18}\text{O}_{\text{precip}}$, with more negative $\delta^{18}\text{O}_{\text{precip}}$ in areas experiencing increased precipitation and vice versa; in this way, the precipitation amount effect opposes the temperature effect. In observations and in the iLME, negative NAO-precipitation amount correlations corresponded with positive $\text{NAO}-\delta^{18}\text{O}_{\text{precip}}$ correlations over the Azores, the subtropical Atlantic, and the tropical Pacific, consistent with an amount effect (Fig. 4, 5b). Changes in local precipitation amount as well as upstream fractionation during anomalous transport (Fig. 5c) can therefore explain the far reach of the NAO in these lower-latitude regions.

Interestingly, the $\text{NAO}-\delta^{18}\text{O}_{\text{precip}}$ correlation over Europe is uniformly positive, despite the canonical north-south contrast in the NAO’s influence on temperature and precipitation (Fig. 5a-b). This likely reflects a latitudinal difference in the primary controls on $\delta^{18}\text{O}_{\text{precip}}$, and thus the $\text{NAO}-\delta^{18}\text{O}_{\text{precip}}$ relationship, across the continent. A positive, direct relationship with temperature can explain NAO-driven $\delta^{18}\text{O}_{\text{precip}}$ in northern Europe and Scandinavia: Positive NAO phases bring warm conditions to this region, which translates to higher $\delta^{18}\text{O}_{\text{precip}}$ (Fig. 4, 5a). Conversely, the negative relationship with precipitation amount can explain NAO-driven $\delta^{18}\text{O}_{\text{precip}}$ in southern Europe. There, positive NAO phases reduce precipitation, resulting in higher $\delta^{18}\text{O}_{\text{precip}}$ values (Fig. 4, 5b). In both regions, therefore, positive (negative) NAO conditions produce higher (lower) $\delta^{18}\text{O}_{\text{precip}}$ values, resulting in a positive correlation between the NAO and $\delta^{18}\text{O}_{\text{precip}}$ across the continent. Previous studies have relied on north-south gradients in European precipitation to reconstruct the NAO (e.g., Trouet et al., 2009). While this is valid for precipitation-driven proxies, our results indicate that studies utilizing $\delta^{18}\text{O}_{\text{precip}}$ -based proxies must be careful to not presume a north-south gradient in $\delta^{18}\text{O}_{\text{precip}}$, because the drivers of $\text{NAO}-\delta^{18}\text{O}_{\text{precip}}$ relationships are spatially variable across Europe.

4.2 NAO teleconnections with South and Central Asia



The positive correlations between the NAO_{Vinter} index and wood cellulose records from the Himalayas and Tibetan Plateau and are strong enough that our NAO reconstructions perform best when they are included. We suggest that the winter $NAO-\delta^{18}O_{wood}$ relationship arises from the combined influence of temperature, precipitation, and changes in moisture source and transport as they are integrated across seasons in the wood cellulose. During winter, the westerlies intensify and flow south of the Tibetan Plateau, bringing moisture to the region from the eastern Mediterranean and western Central Asia (Liu et al., 2017; Schiemann et al., 2009). However, because the eastern Mediterranean and western Central Asia are less humid during positive NAO years, upstream winter IVT is weaker, bringing less winter moisture to the Himalayas and Tibetan Plateau from these distal, westerly moisture sources (Fig. S6). Compared with local sources, moisture imported from distal sources should have lower $\delta^{18}O$ from rainout along the transport path. We speculate that the reduction in imported moisture during positive NAO years would result in higher $\delta^{18}O$ of winter precipitation, contributing to positive correlations between the winter NAO and the $\delta^{18}O$ in wood cellulose records over long timescales.

The Tibetan plateau generally lacks observational $\delta^{18}O_{precip}$ datasets that are long and continuous enough to rigorously evaluate the regional $NAO-\delta^{18}O_{precip}$ relationships, but one station from Lhasa with discontinuous coverage between 1994–2006 CE shows the NAO is significantly negatively correlated with winter temperature and significantly positively correlated with winter precipitation amount (Yao et al., 2013; Table S1). At Lhasa, colder winter temperatures are associated with more negative $\delta^{18}O_{precip}$, whereas increased winter precipitation is associated with more positive $\delta^{18}O_{precip}$ (opposite to the traditional “amount effect”; Dansgaard, 1964) (Table S1). Thus, during the colder and wetter winters of positive NAO years, the competing influences on $\delta^{18}O_{precip}$ result in a weakly positive, though not significant, correlation between the winter NAO and $\delta^{18}O_{precip}$. While additional, continuous station data would be required to better evaluate $NAO-\delta^{18}O_{precip}$ relationships in the Tibetan Plateau, multiple studies from central Asia have observed NAO correlations with $\delta^{18}O_{wood}$ (Liu et al., 2009, 2015; Xu et al., 2021, 2019), supporting the connection which we believe is best explained through moisture source and transport changes.

Like observations, the iLME also shows significant negative correlations between the NAO and precipitation to the northwest (upstream) of the Tibetan Plateau, suggesting drier upstream conditions during positive NAO years, as well as significant positive correlations with $\delta^{18}O_{precip}$ (Fig. 4, 5c). However, the relationship between the winter NAO_{iLME} and surface air temperature over the Tibetan Plateau is opposite that of observations (Fig. 5a). The Himalayas and the Tibetan Plateau are notoriously challenging to resolve in lower-resolution climate models such as that used for the iLME, and contribute to large local biases in precipitation amount, seasonality, moisture source (Li et al., 2022; Lin et al., 2018), and winter $\delta^{18}O_{precip}$ (Gao et al., 2011). We must therefore use caution in interpreting the iLME results local to the Tibetan Plateau and ultimately suggest that reduced influx of depleted moisture from distal sources leads to overall higher $\delta^{18}O$ values across the Tibetan Plateau during positive NAO years, contributing to the relationship observed in the wood cellulose $\delta^{18}O$ records. Longer, continuous station data (>10 years) paired with higher-resolution simulations and proxy system models are needed to further test these mechanisms.

We note that these mechanisms are distinct from previous interpretations that the $NAO-\delta^{18}O_{wood}$ relationship arises from teleconnections between the summer NAO and the Indian Summer Monsoon (ISM) (Sano et al., 2013; Wernicke et al., 2017; Xu et al., 2018). The positive NAO-ISM teleconnection produces a negative $NAO-\delta^{18}O_{wood}$ relationship largely via the amount effect (Bamzai and Shukla, 1999; Rajeevan, 2002; Raman and Maliekal, 1985; Robock et al., 2003), which cannot explain the positive correlation that we observe. The positive winter $NAO_{Vinter}-\delta^{18}O_{wood}$ correlation that we observe, and the Lhasa station data suggest that central Asian $\delta^{18}O_{precip}$ increases following positive winter NAO (Fig. 1, 4). We therefore conclude that while the NAO-ISM teleconnection is important for summer $\delta^{18}O_{precip}$, the winter NAO’s



410 influence on winter $\delta^{18}\text{O}_{\text{precip}}$ strongly influences $\delta^{18}\text{O}_{\text{wood}}$ in locations where snowmelt plays a substantial
411 role during the growing season.

412 **4.3 Low frequency variability in the NAO reconstruction**

413 In our reconstruction, we see strong evidence for multidecadal variability of the NAO (Fig. 6a), which has
414 previously been debated, but also that there is nonstationarity in its strength over the last millennium.
415 Significant decadal and multidecadal variability persists during the Medieval Climate Anomaly (MCA)
416 from ca. 1000–1250 CE and then weakens during the early Little Ice Age (LIA), especially between ca.
417 1300–1700 CE, before increasing again in the final 300 years of the millennium. We argue that water
418 isotope-based proxy records used in our reconstruction integrate climate processes on broad spatiotemporal
419 scales, and therefore are well-poised to capture decadal or longer scale signals that can be missed by proxy
420 systems like tree ring width and density, which are more sensitive to local high frequency variability (Ault
421 et al., 2013; Dee et al., 2017; Moerman et al., 2013).

422 The nonstationary multidecadal variability in our reconstruction is not simply an artifact of changing proxy
423 types and locations through the last millennium. Changes in proxy types could in theory be particularly
424 important after 1600 CE, when many wood cellulose records become available; wood cellulose records
425 have been suggested as biased towards high-frequencies (Dee et al., 2017). However, multidecadal
426 variability is also evident in the wavelet decompositions performed on proxy-specific NAO reconstructions
427 (Fig. S5). Furthermore, the wood cellulose records that do have coverage between ca. 1150–1300 CE (Fig.
428 S5b) also share the increased multidecadal variability reflected in the ice core-based (Fig. S5a) and full
429 NAO reconstructions (Fig. 6). Moreover, NAO variability is strong across scales during the MCA when
430 changes in record availability are gradual, and, more generally, the timing of nonstationarity does not
431 coincide with changes in record availability (Fig. 2b, 6).

432 Nonstationarity in the variability of the NAO across scales through the last millennium is also evident in
433 other NAO reconstructions, but the robustness of low frequency variability has been debated. Landmark
434 reconstructions including Ortega et al. (2017) and Trouet et al. (2009) showed extensive low frequency
435 variability throughout the last millennium, while Cook et al. (2002) and Cook et al. (2019) argued that NAO
436 variability during the last millennium is more consistent with “white noise”. That said, closer inspection of
437 the power spectrum presented in Cook et al. (2019) also shows similar nonstationarity to our NAO
438 reconstruction, with high spectral power in multidecadal bands during the MCA (ca. 950–1300 CE), which
439 then decreases during the mid-millennium and LIA.

440 Nonstationary multidecadal NAO variability during the last millennium therefore appears to be robust. We
441 hypothesize that it arises from the NAO’s interactions with changing latitudinal gradients in Northern
442 Hemisphere temperature, and specifically in the state of the Atlantic Ocean. Latitudinal gradients in sea
443 surface temperature between the tropical and high latitude North Atlantic determine the strength and
444 position of the Azores High and Icelandic Low. Warmer Northern Hemisphere temperatures during the
445 MCA, for example, corresponded with a weakened latitudinal temperature gradient (Li et al., 2013), which
446 may have enhanced decadal to multidecadal variability in the NAO (e.g., Wang et al., 2017). More broadly,
447 it is difficult to reconcile climate shifts across Europe and North America between the MCA and LIA
448 (Edwards et al., 2017; Goosse et al., 2012), and explanations often invoke minor changes in solar and
449 volcanic forcing that were then amplified by internal variability (Goosse et al., 2005; Graham et al., 2011).
450 Better understanding the role for these forcings in multidecadal variability of the NAO, and its
451 nonstationarity from the MCA to LIA, should be a priority (Birkel et al., 2018; Fernandez et al., 2025;
452 Otterå et al., 2010).



It should be noted that the mechanisms underlying climate variability during the majority of the last millennium are quite different from those responsible for modern anthropogenic warming (Goosse et al., 2012), as the magnitude of anthropogenic greenhouse gas forcing far outweighs the magnitude of natural forcings (Kuzmina et al., 2005; Stephenson et al., 2006). The positive trend and increase in significant spectral power across interannual, decadal, multidecadal, and centennial timescales in the industrial era of our reconstruction are suggestive of amplification of variability in Northern Hemisphere atmospheric circulation as a response to anthropogenic climate change (Gillett et al., 2002, 2003; Moore et al., 2017).

The multidecadal variability in the proxy reconstruction is not reproduced in the NAO index derived from the iCESM iLME simulations. This discrepancy aligns with previously documented mismatches between the spectral characteristics of model simulations and those of proxies (Ault et al., 2013; Dee et al., 2017; Franke et al., 2013). Recent work does find multidecadal variability in a spectral analysis of the North Atlantic region in the Last Millennium Ensemble, though high power at multidecadal timescales was limited to periods with major volcanic eruptions and absent from purely internal variability (Fernandez et al., 2025). The fundamental cause of this discrepancy between reconstructions and models—whether due to inherent biases in the models, limitations of the proxies themselves, or a combination of both—remains unresolved.

5.0 Conclusions

Water isotope-based proxies capture the broad range of spatial and temporal impacts of the NAO because they integrate temperature responses across Greenland and Northern Europe, local precipitation amount responses over the Iberian Peninsula and Southern Europe, and moisture source and transport responses in teleconnected regions like South Asia. These relationships explain the skill of our water isotope-based NAO reconstruction, especially when leveraging proxy data from teleconnected regions outside the North Atlantic such as Asia. Our NAO reconstruction reveals strong but nonstationary multidecadal variability across much of the last millennium and future work should evaluate the mechanisms by which external and internal mechanisms affect the timescales of variability in the NAO. Importantly, iCESM (like other models) underestimates the NAO's variability on multidecadal timescales in the reconstruction, suggesting that multidecadal variability could also be underestimated in projections of future climate change. Accounting for low-frequency variability in the NAO as illustrated here will be critical for assessing the risk of NAO impacts to temperature and precipitation across the North Atlantic region in the future.

Data Availability

Data used in this study are publicly available. The Iso2k database is available in R, Matlab, and Python serializations at https://lipdverse.org/iso2k/current_version/. The GNIP data are available at <https://www.iaea.org/services/networks/gnip>. The iCESM Last Millennium Ensemble members are available at <https://rda.ucar.edu/>.

Author Contributions

AAF, BLK, and SC conceptualized the research. AAF performed technical analysis, visualization, and original draft writing. BLK and SC provided supervision, conceptualization, methodology, writing review and editing. BLK contributed the funding sources.

Competing Interests

The authors declare that they have no conflict of interest.

Acknowledgements



We acknowledge the CESM1 (CAM5) Last Millennium Ensemble Community Project and supercomputing resources provided by NSF/CISL/Yellowstone. We also thank Georgy Falster (Australian National University, Australia) and Alex Thompson (Washington University in St. Louis, USA) for help with data acquisition and analysis.

Financial Support

Support for this project was provided by NSF-AGS1805141 and a David and Lucile Packard Foundation Fellowship in Science and Engineering to B. Konecky.

References

- Alley, W. M.: The Palmer Drought Severity Index: Limitations and Assumptions, *J. Climate Appl. Meteor.*, 23, 1100–1109, [https://doi.org/10.1175/1520-0450\(1984\)023%253C1100:TPDSIL%253E2.0.CO;2](https://doi.org/10.1175/1520-0450(1984)023%253C1100:TPDSIL%253E2.0.CO;2), 1984.
- Ault, T. R., Cole, J. E., Overpeck, J. T., Pederson, G. T., St. George, S., Otto-Bliesner, B., Woodhouse, C. A., and Deser, C.: The Continuum of Hydroclimate Variability in Western North America during the Last Millennium, *Journal of Climate*, 26, 5863–5878, <https://doi.org/10.1175/JCLI-D-11-00732.1>, 2013.
- Baldini, L. M., McDermott, F., Foley, A. M., and Baldani, J. U. L.: Spatial variability in the European winter precipitation δ 18O-NAO relationship: Implications for reconstructing NAO-mode climate variability in the Holocene, *Geophysical Research Letters*, 35, <https://doi.org/10.1029/2007GL032027>, 2008.
- Bamzai, A. S. and Shukla, J.: Relation between Eurasian snow cover, snow depth, and the Indian summer monsoon: An observational study, *Journal of Climate*, 12, 3117–3132, [https://doi.org/10.1175/1520-0442\(1999\)012%253C3117:RBESCS%253E2.0.CO;2](https://doi.org/10.1175/1520-0442(1999)012%253C3117:RBESCS%253E2.0.CO;2), 1999.
- Birkel, S. D., Mayewski, P. A., Maasch, K. A., Kurbatov, A. V., and Lyon, B.: Evidence for a volcanic underpinning of the Atlantic multidecadal oscillation, *npj Clim Atmos Sci*, 1, 24, <https://doi.org/10.1038/s41612-018-0036-6>, 2018.
- Bowen, G. J., Cai, Z., Fiorella, R. P., and Putman, A. L.: Isotopes in the Water Cycle: Regional- to Global-Scale Patterns and Applications, *Annu. Rev. Earth Planet. Sci.*, 47, 453–479, <https://doi.org/10.1146/annurev-earth-053018-060220>, 2019.
- Brady, E., Stevenson, S., Bailey, D., Liu, Z., Noone, D., Nusbaumer, J., Otto-Bliesner, B. L., Tabor, C., Tomas, R., Wong, T., Zhang, J., and Zhu, J.: The Connected Isotopic Water Cycle in the Community Earth System Model Version 1, *Journal of Advances in Modeling Earth Systems*, 11, 2547–2566, <https://doi.org/10.1029/2019MS001663>, 2019.
- Brittingham, A., Petrosyan, Z., Hepburn, J. C., Richards, M. P., Hren, M. T., and Hartman, G.: Influence of the North Atlantic Oscillation on δ D and δ 18O in meteoric water in the Armenian Highland, *Journal of Hydrology*, 575, 513–522, <https://doi.org/10.1016/j.jhydrol.2019.05.064>, 2019.
- Casanueva, A., Rodríguez-Puebla, C., Frías, M. D., and González-Reviriego, N.: Variability of extreme precipitation over Europe and its relationships with teleconnection patterns, *Hydrology and Earth System Sciences*, 18, 709–725, <https://doi.org/10.5194/hess-18-709-2014>, 2014.



- 530 Comas-Bru, L., McDermott, F., and Werner, M.: The effect of the East Atlantic pattern on the
531 precipitation $\delta^{18}\text{O}$ -NAO relationship in Europe, *Climate Dynamics*, 47, 2059–2069,
532 <https://doi.org/10.1007/s00382-015-2950-1>, 2016.
- 533 Compo, G. P., Whitaker, J. S., Sardeshmukh, P. D., Matsui, N., Allan, R. J., Yin, X., Gleason, B. E.,
534 Vose, R. S., Rutledge, G., Bessemoulin, P., Brönnimann, S., Brunet, M., Crouthamel, R. I., Grant, A. N.,
535 Groisman, P. Y., Jones, P. D., Kruk, M. C., Kruger, A. C., Marshall, G. J., Maugeri, M., Mok, H. Y.,
536 Nordli, Ø., Ross, T. F., Trigo, R. M., Wang, X. L., Woodruff, S. D., and Worley, S. J.: The Twentieth
537 Century Reanalysis Project, *Quart J Royal Meteorol Soc*, 137, 1–28, <https://doi.org/10.1002/qj.776>, 2011.
- 538 Cook, E. R., D'Arrigo, R. D., and Mann, M. E.: A well-verified, multiproxy reconstruction of the winter
539 North Atlantic Oscillation index since A.D. 1400, *Journal of Climate*, 15, 1754–1764,
540 [https://doi.org/10.1175/1520-0442\(2002\)015%253C1754:AWVMRO%253E2.0.CO;2](https://doi.org/10.1175/1520-0442(2002)015%253C1754:AWVMRO%253E2.0.CO;2), 2002.
- 541 Cook, E. R., Kushnir, Y., Smerdon, J. E., Williams, A. P., Anchukaitis, K. J., and Wahl, E. R.: A Euro-
542 Mediterranean tree-ring reconstruction of the winter NAO index since 910 C.E., *Climate Dynamics*, 53,
543 1567–1580, <https://doi.org/10.1007/s00382-019-04696-2>, 2019.
- 544 Dansgaard, W.: Stable isotopes in precipitation, *Tellus*, 16, 436–468,
545 <https://doi.org/10.3402/tellusa.v16i4.8993>, 1964.
- 546 Dee, S. G., Parsons, L. A., Loope, G. R., Overpeck, J. T., Ault, T. R., and Emile-Geay, J.: Improved
547 spectral comparisons of paleoclimate models and observations via proxy system modeling: Implications
548 for multi-decadal variability, *Earth and Planetary Science Letters*, 476, 34–46,
549 <https://doi.org/10.1016/j.epsl.2017.07.036>, 2017.
- 550 Deininger, M., Werner, M., and McDermott, F.: North Atlantic Oscillation controls on oxygen and
551 hydrogen isotope gradients in winter precipitation across Europe; Implications for palaeoclimate studies,
552 *Climate of the Past*, 12, 2127–2143, <https://doi.org/10.5194/cp-12-2127-2016>, 2016.
- 553 Edwards, T. W. D., Hammarlund, D., Newton, B. W., Sjolte, J., Linderson, H., Sturm, C., St. Amour, N.
554 A., Bailey, J. N.-L., and Nilsson, A. L.: Seasonal variability in Northern Hemisphere atmospheric
555 circulation during the Medieval Climate Anomaly and the Little Ice Age, *Quaternary Science Reviews*,
556 165, 102–110, <https://doi.org/10.1016/j.quascirev.2017.04.018>, 2017.
- 557 Felis, T., Pätzold, J., Loya, Y., Fine, M., Nawar, A. H., and Wefer, G.: A coral oxygen isotope record
558 from the northern Red Sea documenting NAO, ENSO, and North Pacific teleconnections on Middle East
559 climate variability since the year 1750, *Paleoceanography*, 15, 679–694,
560 <https://doi.org/10.1029/1999PA000477>, 2000.
- 561 Fernandez, A., Steinman, B. A., Mann, M. E., and Christiansen, S. A.: Multidecadal Temperature
562 Variability in the Community Earth System Model Last Millennium Ensemble, *Geophysical Research*
563 *Letters*, 52, e2024GL113393, <https://doi.org/10.1029/2024GL113393>, 2025.
- 564 Franke, J., Frank, D., Raible, C. C., Esper, J., and Brönnimann, S.: Spectral biases in tree-ring climate
565 proxies, *Nature Clim Change*, 3, 360–364, <https://doi.org/10.1038/nclimate1816>, 2013.
- 566 Galewsky, J., Steen-Larsen, H. C., Field, R. D., Worden, J., Risi, C., and Schneider, M.: Stable isotopes
567 in atmospheric water vapor and applications to the hydrologic cycle, *Reviews of Geophysics*, 54, 809–
568 865, <https://doi.org/10.1002/2015RG000512>, 2016.



- 569 Gao, J., Masson-Delmotte, V., Yao, T., Tian, L., Risi, C., and Hoffmann, G.: Precipitation Water Stable
570 Isotopes in the South Tibetan Plateau: Observations and Modeling*, *Journal of Climate*, 24, 3161–3178,
571 <https://doi.org/10.1175/2010JCLI3736.1>, 2011.
- 572 Gillett, N. P., Allen, M. R., McDonald, R. E., Senior, C. A., Shindell, D. T., and Schmidt, G. A.: How lin-
573 ear is the Arctic Oscillation response to greenhouse gases?, *J.-Geophys.-Res.*, 107,
574 <https://doi.org/10.1029/2001JD000589>, 2002.
- 575 Gillett, N. P., Graf, H. F., and Osborn, T. J.: Climate change and the North Atlantic Oscillation, in: *Geo-*
576 *physical Monograph Series*, vol. 134, edited by: Hurrell, J. W., Kushnir, Y., Ottersen, G., and Visbeck,
577 M., American Geophysical Union, Washington, D. C., 193–209, <https://doi.org/10.1029/134GM09>, 2003.
- 578 Goosse, H., Renssen, H., Timmermann, A., and Bradley, R. S.: Internal and forced climate variability
579 during the last millennium: a model-data comparison using ensemble simulations, *Quaternary Science*
580 *Reviews*, 24, 1345–1360, <https://doi.org/10.1016/j.quascirev.2004.12.009>, 2005.
- 581 Goosse, H., Cresspin, E., Dubinkina, S., Loutre, M.-F., Mann, M. E., Renssen, H., Sallaz-Damaz, Y., and
582 Shindell, D.: The role of forcing and internal dynamics in explaining the “Medieval Climate Anomaly,”
583 *Clim Dyn*, 39, 2847–2866, <https://doi.org/10.1007/s00382-012-1297-0>, 2012.
- 584 Graham, N. E., Ammann, C. M., Fleitmann, D., Cobb, K. M., and Luterbacher, J.: Support for global cli-
585 mate reorganization during the “Medieval Climate Anomaly,” *Clim Dyn*, 37, 1217–1245,
586 <https://doi.org/10.1007/s00382-010-0914-z>, 2011.
- 587 Hernández, A., Sánchez-López, G., Pla-Rabes, S., Comas-Bru, L., Parnell, A., Cahill, N., Geyer, A.,
588 Trigo, R. M., and Giral, S.: A 2,000-year Bayesian NAO reconstruction from the Iberian Peninsula, *Sci-*
589 *entific Reports*, 10, 1–15, <https://doi.org/10.1038/s41598-020-71372-5>, 2020.
- 590 Hurrell, J. W.: Decadal Trends in the North Atlantic Oscillation: Regional Temperatures and Precipita-
591 tion, *Science*, 269, 676–679, 1995.
- 592 Hurrell, J. W. and Deser, C.: North Atlantic climate variability: The role of the North Atlantic Oscillation,
593 *Journal of Marine Systems*, 78, 28–41, <https://doi.org/10.1016/j.jmarsys.2008.11.026>, 2009.
- 594 IAEA/WMO: Global network of isotopes in precipitation (GNIP), 2008.
- 595 Jones, P. D., Jonsson, T., and Wheeler, D.: Extension to the North Atlantic Oscillation using early instru-
596 mental pressure observations from gibraltar and south-west Iceland, *International Journal of Climatology*,
597 17, 1433–1450, [https://doi.org/10.1002/\(sici\)1097-0088\(19971115\)17:13%253C1433::aid-](https://doi.org/10.1002/(sici)1097-0088(19971115)17:13%253C1433::aid-joc203%253E3.3.co;2-g)
598 [joc203%253E3.3.co;2-g](https://doi.org/10.1002/(sici)1097-0088(19971115)17:13%253C1433::aid-joc203%253E3.3.co;2-g), 1997.
- 599 Konecky, B. L., McKay, N. P., Churakova, O. V., Comas-Bru, L., Dassié, E. P., Delong, K. L., Falster, G.
600 M., Fischer, M. J., Jones, M. D., Jonkers, L., Kaufman, D. S., Leduc, G., Managave, S. R., Martrat, B.,
601 Opel, T., Orsi, A. J., Partin, J. W., Sayani, H. R., Thomas, E. K., Thompson, D. M., Tyler, J. J., Abram,
602 N. J., Atwood, A. R., Cartapanis, O., Conroy, J. L., Curran, M. A., Dee, S. G., Deininger, M., Divine, D.
603 V., Kern, Z., Porter, T. J., Stevenson, S. L., von Gunten, L., Braun, K., Carré, M., Incarbona, A., Kaushal,
604 N., Klabe, R. M., Kolus, H. R., Mortyn, P. G., Moy, A. D., Roop, H. A., Sicre, M. A., Yoshimura, K.,
605 Sidorova, O. V. C., Comas-Bru, L., Dassié, P., Delong, K. L., Falster, G. M., Fischer, M. J., and Jones,
606 M. D.: The Iso2k database: A global compilation of paleo- $\delta^{18}\text{O}$ and $\delta^2\text{H}$ records to aid understanding of
607 Common Era climate, *Earth System Science Data*, 12, 1–49, <https://doi.org/10.5194/essd-12-2261-2020>,
608 2020.



- 609 Kozachek, A., Mikhalevko, V., Masson-Delmotte, V., Ekaykin, A., Ginot, P., Kutuzov, S., Legrand, M.,
610 Lipenkov, V., and Preunkert, S.: Large-scale drivers of Caucasus climate variability in meteorological
611 records and Mt El'brus ice cores, *Climate of the Past*, 13, 473–489, [https://doi.org/10.5194/cp-13-473-](https://doi.org/10.5194/cp-13-473-2017)
612 2017, 2017.
- 613 Kuhnert, H., Crüger, T., and Pätzold, J.: NAO signature in a Bermuda coral Sr/Ca record, *Geochemistry,*
614 *Geophysics, Geosystems*, 6, <https://doi.org/10.1029/2004GC000786>, 2005.
- 615 Kuzmina, S. I., Bengtsson, L., Johannessen, O. M., Drange, H., Bobylev, L. P., and Miles, M. W.: The
616 North Atlantic Oscillation and greenhouse-gas forcing, *Geophysical Research Letters*, 32,
617 2004GL021064, <https://doi.org/10.1029/2004GL021064>, 2005.
- 618 Langebroek, P. M., Werner, M., and Lohmann, G.: Climate information imprinted in oxygen-isotopic
619 composition of precipitation in Europe, *Earth and Planetary Science Letters*, 311, 144–154,
620 <https://doi.org/10.1016/j.epsl.2011.08.049>, 2011.
- 621 Lehner, F., Raible, C. C., and Stocker, T. F.: Testing the robustness of a precipitation proxy-based North
622 Atlantic Oscillation reconstruction, *Quaternary Science Reviews*, 45, 85–94,
623 <https://doi.org/10.1016/j.quascirev.2012.04.025>, 2012.
- 624 Li, G., Chen, H., Xu, M., Zhao, C., Zhong, L., Li, R., Fu, Y., and Gao, Y.: Impacts of Topographic Com-
625 plexity on Modeling Moisture Transport and Precipitation over the Tibetan Plateau in Summer, *Adv. At-*
626 *mos. Sci.*, 39, 1151–1166, <https://doi.org/10.1007/s00376-022-1409-7>, 2022.
- 627 Li, J., Sun, C., and Jin, F. F.: NAO implicated as a predictor of Northern Hemisphere mean temperature
628 multidecadal variability, *Geophysical Research Letters*, 40, 5497–5502,
629 <https://doi.org/10.1002/2013GL057877>, 2013.
- 630 Lin, C., Chen, D., Yang, K., and Ou, T.: Impact of model resolution on simulating the water vapor
631 transport through the central Himalayas: implication for models' wet bias over the Tibetan Plateau, *Clim*
632 *Dyn*, 51, 3195–3207, <https://doi.org/10.1007/s00382-018-4074-x>, 2018.
- 633 Liu, H., Liu, X., and Dong, B.: Intraseasonal variability of winter precipitation over central asia and the
634 western tibetan plateau from 1979 to 2013 and its relationship with the North Atlantic Oscillation, *Dy-*
635 *namics of Atmospheres and Oceans*, 79, 31–42, <https://doi.org/10.1016/j.dynatmoce.2017.07.001>, 2017.
- 636 Liu, X., Shao, X., Liang, E., Chen, T., Qin, D., An, W., Xu, G., Sun, W., and Wang, Y.: Climatic signifi-
637 cance of tree-ring $\delta^{18}\text{O}$ in the Qilian Mountains, northwestern China and its relationship to atmospheric
638 circulation patterns, *Chemical Geology*, 268, 147–154, <https://doi.org/10.1016/j.chemgeo.2009.08.005>,
639 2009.
- 640 Liu, X., An, W., Treydte, K., Wang, W., Xu, G., Zeng, X., Wu, G., Wang, B., and Zhang, X.: Pooled ver-
641 sus separate tree-ring δD measurements, and implications for reconstruction of the Arctic Oscillation in
642 northwestern China, *Science of The Total Environment*, 511, 584–594, [https://doi.org/10.1016/j.sci-](https://doi.org/10.1016/j.sci-2015.01.002)
643 [totenv.2015.01.002](https://doi.org/10.1016/j.sci-totenv.2015.01.002), 2015.
- 644 Liu, Y., Chen, H., Wang, H., and Qiu, Y.: The Impact of the NAO on the Delayed Break-Up Date of Lake
645 Ice over the Southern Tibetan Plateau, *Journal of Climate*, 31, 9073–9086, [https://doi.org/10.1175/JCLI-](https://doi.org/10.1175/JCLI-D-18-0197.1)
646 [D-18-0197.1](https://doi.org/10.1175/JCLI-D-18-0197.1), 2018.



- 647 Mann, M. E., Zhang, Z., Hughes, M. K., Bradley, R. S., Miller, S. K., Rutherford, S., and Ni, F.: Proxy-
648 based reconstructions of hemispheric and global surface temperature variations over the past two millen-
649 nia, *Proceedings of the National Academy of Sciences of the United States of America*, 105, 13252–
650 13257, <https://doi.org/10.1073/pnas.0805721105>, 2008.
- 651 Mckay, N., Emile-geay, J., and Khider, D.: GeoChronR – an R package to model , analyze and visualize
652 age-uncertain paleoscientific data, *Geochronology Discussions*, 1–33, 2020.
- 653 Meyers, S. R.: Seeing red in cyclic stratigraphy: Spectral noise estimation for astrochronology,
654 *Paleoceanography*, 27, 1–12, <https://doi.org/10.1029/2012PA002307>, 2012.
- 655 Michel, S., Swingedouw, D., Chavent, M., Ortega, P., Mignot, J., and Khodri, M.: Reconstructing cli-
656 matic modes of variability from proxy records using ClimIndRec version 1.0, *Geoscientific Model Devel-*
657 *opment*, 13, 841–858, <https://doi.org/10.5194/gmd-13-841-2020>, 2020.
- 658 Moerman, J. W., Cobb, K. M., Adkins, J. F., Sodemann, H., Clark, B., and Tuen, A. A.: Diurnal to inter-
659 annual rainfall $\delta^{18}\text{O}$ variations in northern Borneo driven by regional hydrology, *Earth and Planetary Sci-*
660 *ence Letters*, 369–370, 108–119, <https://doi.org/10.1016/j.epsl.2013.03.014>, 2013.
- 661 Moore, G. W. K., Halfar, J., Majeed, H., Adey, W., and Kronz, A.: Amplification of the Atlantic Multide-
662 cadal Oscillation associated with the onset of the industrial-era warming, *Sci Rep*, 7, 40861,
663 <https://doi.org/10.1038/srep40861>, 2017.
- 664 Neukom, R., Gergis, J., Karoly, D. J., Wanner, H., Curran, M., Elbert, J., González-Rouco, F., Linsley, B.
665 K., Moy, A. D., Mundo, I., Raible, C. C., Steig, E. J., Van Ommen, T., Vance, T., Villalba, R., Zinke, J.,
666 and Frank, D.: Inter-hemispheric temperature variability over the past millennium, *Nature Climate*
667 *Change*, 4, 362–367, <https://doi.org/10.1038/nclimate2174>, 2014.
- 668 Nusbaumer, J., Wong, T. E., Bardeen, C., and Noone, D.: Evaluating hydrological processes in the Com-
669 munity Atmosphere Model Version 5 (CAM5) using stable isotope ratios of water, *J Adv Model Earth*
670 *Syst*, 9, 949–977, <https://doi.org/10.1002/2016MS000839>, 2017.
- 671 Ortega, P., Lehner, F., Swingedouw, D., Masson-Delmotte, V., Raible, C. C., Casado, M., and Yiou, P.: A
672 model-tested North Atlantic Oscillation reconstruction for the past millennium, *Nature*, 523, 71–74,
673 <https://doi.org/10.1038/nature14518>, 2015.
- 674 Otterå, O. H., Bentsen, M., Drange, H., and Suo, L.: External forcing as a metronome for Atlantic mul-
675 tidecadal variability, *Nature Geosci*, 3, 688–694, <https://doi.org/10.1038/ngeo955>, 2010.
- 676 Pearson, K.: On lines and planes of closest fit to systems of points in space, *The London, Edinburgh, and*
677 *Dublin Philosophical Magazine and Journal of Science*, 2, 559–572,
678 <https://doi.org/10.1080/14786440109462720>, 1901.
- 679 Puntsg, T., Mitchell, M. J., Campbell, J. L., Klein, E. S., Likens, G. E., and Welker, J. M.: Arctic Vortex
680 changes alter the sources and isotopic values of precipitation in northeastern US, *Scientific Reports*, 6, 1–
681 9, <https://doi.org/10.1038/srep22647>, 2016.
- 682 Putman, A. L. and Bowen, G. J.: Technical Note: A global database of the stable isotopic ratios of mete-
683 oric and terrestrial waters, *Hydrology and Earth System Sciences*, 23, 4389–4396,
684 <https://doi.org/10.5194/hess-23-4389-2019>, 2019.



- 685 Rajeevan, M.: Winter surface pressure anomalies over Eurasia and Indian summer monsoon, *Geophysical*
686 *Research Letters*, 29, 94–1–94–4, <https://doi.org/10.1029/2001GL014363>, 2002.
- 687 Raman, C. R. V. and Maliekal, J. A.: A “northern oscillation” relating northern hemispheric pressure
688 anomalies and the Indian summer monsoon?, *Nature*, 314, 430–432, <https://doi.org/10.1038/314430a0>,
689 1985.
- 690 Robock, A., Mu, M., Vinnikov, K., and Robinson, D.: Land surface conditions over Eurasia and Indian
691 summer monsoon rainfall, *Journal of Geophysical Research: Atmospheres*, 108,
692 <https://doi.org/10.1029/2002jd002286>, 2003.
- 693 Roesch, A. and Schmidbaur, H.: WaveletComp: Computational Wavelet Analysis. R package version 1.1,
694 2018.
- 695 Rozanski, K., Araguás-Araguás, L., and Gonfiantini, R.: Isotopic Patterns in Modern Global Precipitation,
696 *Geophysical Monograph*, 78, 1–37, <https://doi.org/10.1029/GM078p0001>, 1993.
- 697 Sánchez-López, G., Hernández, A., Pla-Rabes, S., Trigo, R. M., Toro, M., Granados, I., Sáez, A., Mas-
698 qué, P., Pueyo, J. J., Rubio-Inglés, M. J., and Giral, S.: Climate reconstruction for the last two millennia
699 in central Iberia: The role of East Atlantic (EA), North Atlantic Oscillation (NAO) and their interplay
700 over the Iberian Peninsula, *Quaternary Science Reviews*, 149, 135–150, <https://doi.org/10.1016/j.quasci-rev.2016.07.021>, 2016.
- 702 Sano, M., Tshering, P., Komori, J., Fujita, K., Xu, C., and Nakatsuka, T.: May–September precipitation in
703 the Bhutan Himalaya since 1743 as reconstructed from tree ring cellulose $\delta^{18}\text{O}$, *JGR Atmospheres*, 118,
704 8399–8410, <https://doi.org/10.1002/jgrd.50664>, 2013.
- 705 Schiemann, R., Lüthi, D., and Schär, C.: Seasonality and interannual variability of the westerley jet in the
706 Tibetan Plateau region, *Journal of Climate*, 22, 2940–2957, <https://doi.org/10.1175/2008JCLI2625.1>,
707 2009.
- 708 Schmutz, C., Luterbacher, J., Gyalistras, D., Xoplaki, E., and Wanner, H.: Can we trust proxy-based NAO
709 index reconstructions?, *Geophysical Research Letters*, 27, 1135–1138,
710 <https://doi.org/10.1029/1999GL011045>, 2000.
- 711 Sodemann, H., Schwierz, C., and Wernli, H.: Interannual variability of Greenland winter precipitation
712 sources: Lagrangian moisture diagnostic and North Atlantic Oscillation influence, *Journal of Geophysical*
713 *Research Atmospheres*, 113, 1–17, <https://doi.org/10.1029/2007JD008503>, 2008.
- 714 Sorrel, P., Popescu, S. M., Klotz, S., Suc, J. P., and Oberhänsli, H.: Climate variability in the Aral Sea ba-
715 sin (Central Asia) during the late Holocene based on vegetation changes, *Quaternary Research*, 67, 357–
716 370, <https://doi.org/10.1016/j.yqres.2006.11.006>, 2007.
- 717 Stephenson, D. B., Pavan, V., Collins, M., Junge, M. M., Quadrelli, R., and Participating CMIP2 Model-
718 ling Groups: North Atlantic Oscillation response to transient greenhouse gas forcing and the impact on
719 European winter climate: a CMIP2 multi-model assessment, *Clim Dyn*, 27, 401–420,
720 <https://doi.org/10.1007/s00382-006-0140-x>, 2006.
- 721 Thomson, D. J.: Spectrum Estimation and Harmonic Analysis, *Proceedings of the IEEE*, 70, 1055–1096,
722 1982.



- 723 Trigo, R., Osborn, T., and Corte-Real, J.: The North Atlantic Oscillation influence on Europe: climate im-
724 pacts and associated physical mechanisms, *Climate Research*, 20, 9–17, <https://doi.org/10.3354/cr020009>,
725 2002.
- 726 Trouet, V., Esper, J., Graham, N. E., Baker, A., Scourse, J. D., and Frank, D. C.: Persistent Positive North
727 Atlantic Oscillation Mode Dominated the Medieval Climate Anomaly, *Science*, 324, 78–80,
728 <https://doi.org/10.1126/science.1166349>, 2009.
- 729 Vachon, R. W., Welker, J. M., White, J. W. C., and Vaughn, B. H.: Moisture source temperatures and
730 precipitation $\delta^{18}\text{O}$ - temperature relationships across the United States, *Water Resources Research*, 46, 1–
731 14, <https://doi.org/10.1029/2009WR008558>, 2010.
- 732 Villarini, G., Smith, J. A., Ntelekos, A. A., and Schwarz, U.: Annual maximum and peaks-over-threshold
733 analyses of daily rainfall accumulations for Austria, *Journal of Geophysical Research Atmospheres*, 116,
734 1–15, <https://doi.org/10.1029/2010JD015038>, 2011.
- 735 Vinther, B. M., Andersen, K. K., Hansen, A. W., Schmith, T., and Jones, P. D.: Improving the Gibrat-
736 tar/Reykjavik NAO index, *Geophysical Research Letters*, 30, 1–4,
737 <https://doi.org/10.1029/2003GL018220>, 2003a.
- 738 Vinther, B. M., Johnsen, S. J., Andersen, K. K., Clausen, H. B., and Hansen, A. W.: NAO signal recorded
739 in the stable isotopes of Greenland ice cores, *Geophysical Research Letters*, 30, 2002GL016193,
740 <https://doi.org/10.1029/2002GL016193>, 2003b.
- 741 Vuille, M. and Werner, M.: Stable isotopes in precipitation recording South American summer monsoon
742 and ENSO variability: Observations and model results, *Climate Dynamics*, 25, 401–413,
743 <https://doi.org/10.1007/s00382-005-0049-9>, 2005.
- 744 Wang, Z., Duan, A., Yang, S., and Ullah, K.: Atmospheric moisture budget and its regulation on the vari-
745 ability of summer precipitation over the tibetan plateau, *Journal of Geophysical Research*, 122, 614–630,
746 <https://doi.org/10.1002/2016JD025515>, 2017.
- 747 Wernicke, J., Hochreuther, P., Griebinger, J., Zhu, H., Wang, L., and Bräuning, A.: Multi-century humid-
748 ity reconstructions from the southeastern Tibetan Plateau inferred from tree-ring $\delta^{18}\text{O}$, *Global and Plane-*
749 *tary Change*, 149, 26–35, <https://doi.org/10.1016/j.gloplacha.2016.12.013>, 2017.
- 750 Woollings, T. and Blackburn, M.: The north Atlantic jet stream under climate change and its relation to
751 the NAO and EA patterns, *Journal of Climate*, 25, 886–902, <https://doi.org/10.1175/JCLI-D-11-00087.1>,
752 2012.
- 753 Woollings, T., Hannachi, A., and Hoskins, B.: Variability of the North Atlantic eddy-driven jet stream,
754 *Quarterly Journal of the Royal Meteorological Society*, 136, 856–868, <https://doi.org/10.1002/qj.625>,
755 2010.
- 756 Woollings, T., Franzke, C., Hodson, D. L. R., Dong, B., Barnes, E. A., Raible, C. C., and Pinto, J. G.:
757 Contrasting interannual and multidecadal NAO variability, *Climate Dynamics*, 45, 539–556,
758 <https://doi.org/10.1007/s00382-014-2237-y>, 2015.
- 759 Woollings, T., Barnes, E., Hoskins, B., Kwon, Y. O., Lee, R. W., Li, C., Madonna, E., McGraw, M., Par-
760 ker, T., Rodrigues, R., Spensberger, C., and Williams, K.: Daily to decadal modulation of jet variability,
761 *Journal of Climate*, 31, 1297–1314, <https://doi.org/10.1175/JCLI-D-17-0286.1>, 2018.



- 762 Xiaoge, X., Zhou, T., and Yu, R.: Increased Tibetan Plateau snow depth: An indicator of the connection
763 between enhanced winter NAO and late-spring tropospheric cooling over East Asia, *Adv. Atmos. Sci.*, 27,
764 788–794, <https://doi.org/10.1007/s00376-009-9071-x>, 2010.
- 765 Xu, C., Sano, M., Dimri, A. P., Ramesh, R., Nakatsuka, T., Shi, F., and Guo, Z.: Decreasing Indian sum-
766 mer monsoon on the northern Indian sub-continent during the last 180 years: evidence from five tree-ring
767 cellulose oxygen isotope chronologies, *Clim. Past*, 14, 653–664, <https://doi.org/10.5194/cp-14-653-2018>,
768 2018.
- 769 Xu, C., Zhao, Q., An, W., Wang, S., Tan, N., Sano, M., Nakatsuka, T., Borhara, K., and Guo, Z.: Tree-
770 ring oxygen isotope across monsoon Asia: Common signal and local influence, *Quaternary Science Re-
771 views*, 269, 107156, <https://doi.org/10.1016/j.quascirev.2021.107156>, 2021.
- 772 Xu, G., Liu, X., Trouet, V., Treydte, K., Wu, G., Chen, T., Sun, W., An, W., Wang, W., Zeng, X., and
773 Qin, D.: Regional drought shifts (1710–2010) in East Central Asia and linkages with atmospheric circula-
774 tion recorded in tree-ring $\delta^{18}\text{O}$, *Clim Dyn*, 52, 713–727, <https://doi.org/10.1007/s00382-018-4215-2>,
775 2019.
- 776 Yao, T., Masson-Delmotte, V., Gao, J., Yu, W., Yang, X., Risi, C., Sturm, C., Werner, M., Zhao, H., He,
777 Y., Ren, W., Tian, L., Shi, C., and Hou, S.: A review of climatic controls on $\delta^{18}\text{O}$ in precipitation over
778 the Tibetan Plateau: Observations and simulations, *Reviews of Geophysics*, 51, 525–548,
779 <https://doi.org/10.1002/rog.20023>, 2013.
- 780 Zanardo, S., Nicotina, L., Hilberts, A. G. J., and Jewson, S. P.: Modulation of Economic Losses From Eu-
781 ropean Floods by the North Atlantic Oscillation, *Geophysical Research Letters*, 46, 2563–2572,
782 <https://doi.org/10.1029/2019GL081956>, 2019.
- 783 Zhu, F., Emile-Geay, J., McKay, N. P., Hakim, G. J., Khider, D., Ault, T. R., Steig, E. J., Dee, S., and
784 Kirchner, J. W.: Climate models can correctly simulate the continuum of global-average temperature vari-
785 ability, *Proceedings of the National Academy of Sciences of the United States of America*, 116, 8728–
786 8733, <https://doi.org/10.1073/pnas.1809959116>, 2019.

787